

# Microstructure and magnetic properties of Mn-Al-C permanent magnets produced by various techniques

Vladimir V. Popov Jr.<sup>1,\*,\*\*</sup>, Fernando Maccari<sup>2,\*\*</sup>, Iliya A. Radulov<sup>2</sup>, Aleksey Kovalevsky<sup>1</sup>, Alexander Katz-Demyanetz<sup>1</sup>, and Menahem Bamberger<sup>3</sup>

<sup>1</sup> Israel Institute of Metals, Technion R&D Foundation, Technion City, Haifa 3200003, Israel

<sup>2</sup> Technical University Darmstadt, Alarich-Weiss-Street 16, Darmstadt 64287, Germany

<sup>3</sup> Department of Materials Science and Engineering, Technion Israel Institute of Technology, Technion City, Haifa 3200003, Israel

Received: 7 February 2021 / Accepted: 14 March 2021

**Abstract.** Bulk  $\text{Mn}_{52}\text{Al}_{46}\text{C}_2$  in  $\tau$ -phase was prepared by vacuum induction melting and used as precursor for the production bulk permanent magnets by suction casting and hot-extrusion. Part of the precursor alloy was mechanically milled into a  $\tau$ -phase powder and used as precursor for production of samples by electron beam melting, hot-compaction and high pressure torsion processes. The microstructure and magnetic properties of all samples were investigated and correlated. It was found that the mechanical deformation enhances coercivity, up to 0.58 T, while the absence of this strain is beneficial for magnetization. Among the observed techniques, hot extrusion and high pressure torsion have shown promising possibilities to further develop Mn-Al-C as permanent magnets. However, it should be taken into account the challenges related to design a proper processing window for hot extrusion and the limitation of HPT regarding the absence of texture.

**Keywords:** Manufacturing methods / permanent magnets / rare earth free magnets / Mn-Al-C alloys

## 1 Introduction

Mn-Al alloys belong to the well-known material systems, which have been intensively studied since the late 60's as perspective candidates for use as permanent magnets (PM) [1,2], but then faded into oblivion after the discovery of the Nd-Fe-B magnets in the 80's [3]. The abrupt increase of the rare earth elements price in 2011, along with the growing demand on permanent magnets, triggered the renewed interest in this material system in the past years [3,4]. This combination of circumstances has motivated many scientists to not only search for novel materials, but also to re-investigate already known materials systems like MnAl and work further on the development of new fabrication techniques, involving novel routes of powder metallurgy [5–7], hot deformation [8–12] and additive manufacturing [13–16] which can provide hard magnetic properties for these non-rare-earth relatively cheap permanent magnets [4].

The MnAl material system is characterized by the use of non-critical elements, low cost and reasonable magnetic properties [2,3,17]. These characteristics are

pointed as crucial to use and develop this material system as “gap magnets” [18,19]. This terminology is adopted to show that this material system has the intrinsic magnetic properties suitable to fill the magnetic performance gap (in the meaning of energy product –  $BH_{max}$ ) between the cheap but low performance ferrites ( $BH_{max} \approx 40 \text{ kJ/m}^3$ ) and the expensive, rare-earth based high performance magnets (N45 grade Nd-Fe-B- $BH_{max} \approx 450 \text{ kJ/m}^3$ ) [20]. The intrinsic properties of the Mn-Al compound show a high anisotropy constant ( $K_1$  of  $1.7 \text{ MJ/m}^3$ ), relatively high anisotropy field ( $H_A$  between 4.0 and 5.5 T), moderate saturation magnetization ( $M_S$  of 0.75 T) which yields in the theoretical value of  $BH_{max} \approx 95 \text{ kJ/m}^3$  [20,21].

The magnetic properties of Mn-Al are related to the solely ferromagnetic metastable phase in this material system, the tetragonal  $\tau$ -phase ( $\text{Ll}_0$  type structure). As a general rule, the processing window has to be design in a way to produce pure ferromagnetic phase in the Mn-Al system in order to maximize magnetization. This can be achieved by two common methods: (i) quenching from the melt or from high temperatures (around  $1100^\circ\text{C}$ ) to stabilize the parent  $\varepsilon$ -phase (hexagonal structure-HCP) followed by annealing at moderate temperatures (around  $500^\circ\text{C}$ ); (ii) high temperature annealing followed by controlled cooling, which results in  $\tau$ -phase nucleation and

\* e-mail: [vvp@technion.ac.il](mailto:vvp@technion.ac.il)

\*\* Both V.V.P. and F.M. equally contributed to this work.

growth during this last step. As mentioned, the ferromagnetic phase is metastable, which means that long annealing times or high temperatures can lead to decomposition of the  $\tau$ -phase and nucleation of the non-magnetic stable  $\gamma_2$  and  $\beta$ -phases [20,22,23]. The formation of the ordered  $L1_0$   $\tau$ -phase, from the parent chemically disordered HCP  $\varepsilon$ -phase, is reported to happen through two main mechanisms: massive and displacive. The first one is associated with diffusional nucleation at the  $\varepsilon$ -phase grain boundaries followed by growth via interphase boundary motion [24]. The latter is related to the shear of HCP atomic planes with short-range diffusion [25]. It can also be the case that these two mechanisms happen simultaneously, as observed by *insitu* experiments at temperatures around 500 °C or above [26]. The growth of the  $\tau$ -phase develops lattice/microstructural defects which affects substantially the magnetic performance, as will be discussed later [24].

To increase the stability of the ferromagnetic phase, carbon is often added as interstitial dopant to the  $\tau$ -phase compositional range,  $Mn_{50+x}Al_{50-x}$  ( $51 \leq x \leq 58$ ), at the expenses of decreasing the Curie temperature ( $T_C$ ) from 630 to 570 K [20,22]. But only phase purity is not a guarantee for optimized magnetic properties, since different manufacturing processes affect the microstructure and, consequently, the extrinsic magnetic properties.

Different studies have shown the complex relation between the several types of microstructural defects of  $\tau$ -MnAl phase and the magnetic properties, in terms of remanence, coercivity and, consequently, the  $BH_{max}$  value [10,21,27–32]. Among the possible defects in this material system, the existence of twin boundaries is often related to one of the major difficulties to obtain highly textured samples and improved remanence in Mn-Al magnets [31]. This is linked to the high density of twin variants created during the  $\tau$ -phase formation, which will prevent the achievement high degree of texture along the easy magnetization axis since randomly multi-variant grains will be formed. Moreover, in addition to twin boundaries, other defects and metallurgical variables which were reported, namely: stacking faults, antiphase boundaries, dislocations, grain size and lattice strain; are related and affect coercivity, as reported in the literature [10,21,31,32]. The effect of each specific defect on the magnetic properties is still under investigation, as different characterization techniques are necessary to obtain qualitatively and/or quantitatively data about the density and distribution of these defects. Furthermore, these microstructural features are very often reported to coexist, which increase the challenge to understand the coercivity mechanism in  $\tau$ -Mn-Al-based compounds.

Based on these factors, a complete understand of the processing route on the phase stability, microstructure and magnetic properties are indispensable to optimize the Mn-Al material system to be suitable for permanent magnet applications. Therefore, this present work is focused on the use of five different processing techniques for production of Mn-Al-C bulk samples and the correlation between microstructure and magnetic properties for each of these processes.

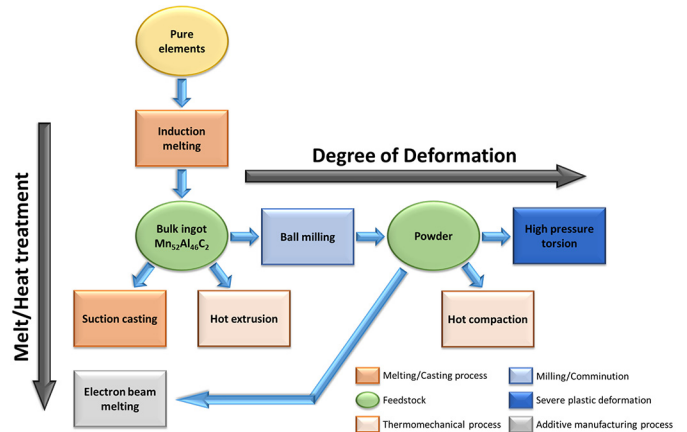


Fig. 1. Overview of the methods used to prepare Mn-Al-C based permanent magnets.

## 2 Sample synthesis and characterization

In the following subsections will be given experimental details of the different processing routes discussed in this work, according to the schematic presented in Figure 1. The master alloy composition,  $Mn_{52}Al_{46}C_2$ , chosen to perform these processes was based on the low ratio between Mn and Al atoms, to avoid decrease in magnetization from the Mn-Mn antiferromagnetic interaction, and interstitial C doping to prevent decomposition of the metastable hard magnetic  $L1_0$   $\tau$ -phase.

### 2.1 Synthesis of the bulk precursor alloy

#### 2.1.1 Vacuum induction melting

Vacuum induction melting (VIM) followed by casting into graphite crucible is a well-known fabrication technique, especially for Mn-Al production [2].  $Mn_{52}Al_{46}C_2$  alloy was prepared by melting pure elements (purity above 99 wt. %) using a single chamber vacuum induction melting furnace (Consarc Corp.). Before melting, the chamber purged with argon 5 times in order to reduce the oxygen content to a minimum level. The melting occurred under protective atmosphere of Ar (purity of 99.999%) and the alloy was kept in a molten state for 2 h for homogenization before casting into a graphite crucible. The so obtained bulk alloy was further characterized and used as a precursor in all subsequent processing routes, as shown in Figure 1, ensuring the same chemical composition for a direct comparison between the processes.

#### 2.1.2 Suction casting

Part of the VIM Mn-Al-C bulk sample was subject to arc melting and, when in molten state, the alloy was rapidly “sucked” into a cylindrical cooled copper mold of 10 mm diameter. This is a method of casting that ensure high 95 cooling rates, in the order of  $10^3$  Ks<sup>-1</sup>, and allows to obtain microstructural refinement and non-equilibrium phases. This technique has been reported for different intermetallic

rare-earth based compounds [33–35]. However, there are no reports of the use of suction casting for Mn-Al, to the best of authors knowledge. The suction cast samples were subjected to the following heat treatment procedure: annealing for 72 h at 1100 °C, followed by water quenching and subsequently annealing for 30 min at 550 °C.

### 2.1.3 Hot deformation/hot extrusion

The effect of hot extrusion was investigated by Matsushita Electrical Industrial company in 1977, it was reported values of  $H_C = 0.30$  T,  $(BH)_{max} \approx 56$  kJ/m<sup>3</sup> for Mn-Al-C compound [36]. Texture along the hot extrusion direction was observed from the anisotropy behavior in the magnetic measurements. This result still remains as state of the art in terms of magnetic performance and difficulties on reproducing it were reported in literature (references). Only recently Feng et al. reported similar values  $(BH)_{max} \approx 46$  kJ/m<sup>3</sup> [37]. In this comprehensive study, it was highlighted the role of Ni-doping on the improving the plasticity of Mn-Al-C, which is imperative for the hot extrusion process.

A press (Beckwood corp.), with tools heated up to 550 °C, was used for the extrusion process. The diameter of the die used was 25 mm while the initial diameter of the samples was 50 mm, resulting in a ratio of the starting and final cross section area of 4. Prior extrusion the precursor alloy was heated up to 500 °C and kept at this temperature for ca. 20 min. Afterwards the preheated alloy was placed into the press and pressure of up to 225 MPa was applied. However, due to the rigid behaviour of the intermetallic phase at this temperature, the applied pressure was not sufficient to successfully complete the extrusion process.

Even though a small volume of the sample was extruded, a section of this volume was used for further characterization.

## 2.2 Synthesis of the powder precursor alloy

Various techniques have been previously applied to prepare Mn-Al based powder precursor for permanent magnets, including mechanical alloying, gas atomization and mechanical milling etc. [5–7,17,38,39]. Among this methods, mechanical milling (MM) seems to be the most cost-effective and efficient approach for preparation of powder with enhanced coercivity. Therefore, powder was produced by mechanical milling of the VIM obtained Mn-Al-C alloy, by using a planetary ball mill Fritsch-Pulverisette 6. The milling was done in protective gas atmosphere, for 2 h at rotation speed of 250 RPM, using 10:1 ball to powder mass ratio, and 10 mm hardened steel balls.

### 2.2.1 Hot compaction

After milling, the randomly shaped powder and flake like particles, with  $D_{90} \leq 100$  μm was obtained. The powder was sieved and separated in fraction by particles sizes. The fraction with particle size below 100 μm was used for hot compaction. The hot compaction has been performed using a standard hydraulic hot press machine and closed die with

inner diameter of 300 mm and height (after compaction) of 800 mm. The compaction was done at pressure of 150 MPa and die temperature of 450 °C under protective argon atmosphere with holding time of 20 min.

### 2.2.2 High pressure torsion

The influence of plastic deformation as well as of crystal defects related to crystals plasticity on the formation magnetic properties of Mn-Al based alloys was intensively studied through recent years [30,31,40,41]. The high pressure torsion (HPT – Walter Klements GmbH) process was used to compact and deform  $\tau$ -phase Mn-Al-C powder (particle size below 80 μm) into disc shaped samples of 10 mm diameter and 1 mm height. The pressure used was 4 GPa and 50 revolutions were applied with 1 RPM. The process was performed at room temperature and the tools were kept below 50 °C during the process.

During the HPT process, the strain generated within the sample is proportional to the radius, which means that the edges of the disc will be higher deformed than the center, leading to an inhomogeneous microstructure and, in this case, a magnetic properties gradient [42]. For this reason, we evaluated three regions of the sample: center ( $R_0$ ), half radius ( $R_{0.5}$ ) and on the edge ( $R_1$ ).

### 2.2.3 Additive manufacturing

An Arcam EBM A2 machine (Arcam EBM, Sweden) was used for the additive manufacturing process. The EBM system has reduced working volume, optimized for the experiments with small powder batches e.g., for testing new alloys [43]. Processing parameters used: layer thickness 100 μm; line offset 100 μm; maximum beam current (EB) 30 mA and average chamber temperature of 830 °C. More details about the processing and optimization can be found in [15].

## 2.3 Characterisation techniques

### 2.3.1 SEM/Kerr microscopy

To investigate the present phases and microstructure, the samples were analyzed using scanning electron microscope (SEM – Tescan VEGA 3 and FEG-SEM JEOL JSM-7600F) with backscattered electrons (BSE) detector. Energy-dispersive X-ray spectroscopy (EDS) measurements were performed to quantify chemical composition of the present phases. In addition, EDS measurements were taken in larger portions of the sample (area scans) to ensure the Mn/Al ratio was preserved after each processing technique. In all cases, the overall error/deviation from the initial aimed stoichiometry was around 1 at%, within the limits of the EDS detector. The carbon content was evaluated qualitatively by comparing the different samples, since the quantitative determination through EDS is challenging and can be influenced by different measurements artifacts (specimen surface or SEM chamber contamination).

The magnetic domain structures were observed by magneto optical Kerr effect (MOKE) microscopy (Zeiss Axio Imager.D2m evico magnetics GmbH).

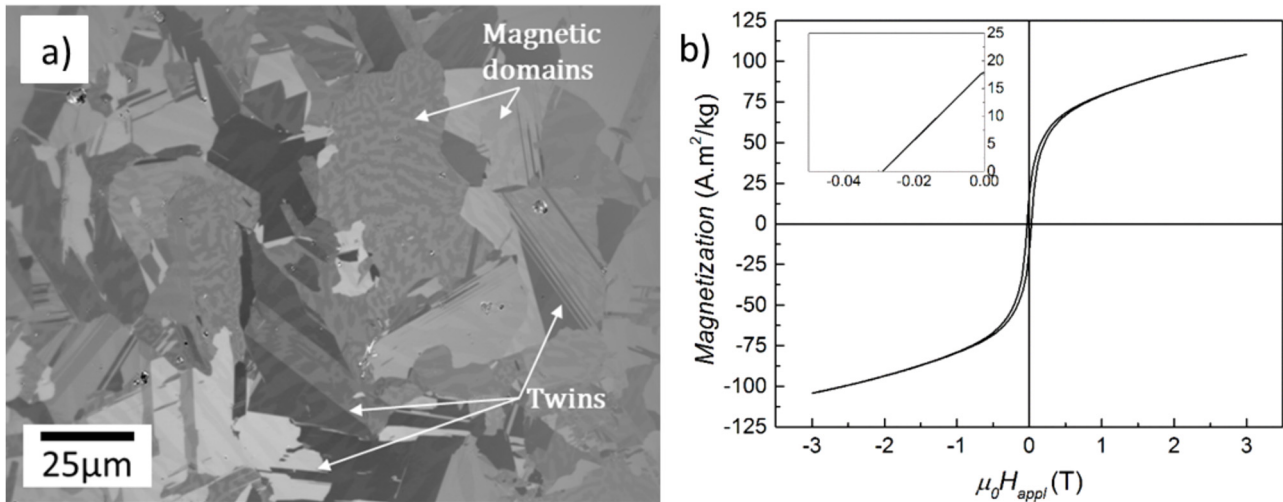


**Fig. 2.** Kerr micrograph (a) and magnetization measurement (b) of the VIM casted Mn-Al-C sample. The microstructure shows pure  $\tau$ -phase with twin boundaries and the magnetic domain structure.

### 2.3.2 Magnetisation measurements

Isothermal magnetization measurements were performed using PPMS-VSM (Quantum Design PPMS-14), at room temperature, under applied magnetic field up to 3 T. No corrections regarding demagnetizing factor were made.

### 2.3.3 Transmission electron microscopy-TEM

Prior to TEM analysis, lamellas were prepared using plasma FIB (TescanS9000X) from samples in the VIM, powder and HPT states. The TEM TitanThemis G2 60-300 (FEI/Thermo Fisher) with aberration correction and rapid camera with 4K resolution was used to analyze the lamellas.

## 3 Results and discussion

### 3.1 Vacuum induction melting (VIM)

The sample after VIM shows ferromagnetic behavior, as presented in Figure 2b with relatively high magnetization at 3 T applied field ( $M_{3T}$ ) of  $100 \text{ A} \cdot \text{m}^2/\text{kg}$ , in agreement with the microstructure shown in Figure 2a, in which only  $\tau$ -phase is observed. It is important to notice the small value of coercivity ( $H_C < 0.03 \text{ T}$ ), which is directly related with the coarse microstructure with high density of twin boundaries and the absence of defects which pin the domain wall motion, as similarly reported by [9,31]. The resultant phase/microstructure arises from the casting process, where the cooling is not fast enough to stabilize the high temperature  $\epsilon$ -phase and not slow to promote the stable  $\gamma_2$ - and  $\beta$ -phases. Since an intermediate cooling rate is achieved during VIM, the nucleation and growth of the  $\tau$ -phase was achieved, leading to a single-phase sample.

### 3.2 Powder preparation – ball milling

$\text{Mn}_{52}\text{Al}_{46}\text{C}_2$  powder was prepared from the VIM bulk precursor, through ball milling, for further processing routes. As can be seen from the SEM-BSE image on Figure 3a, the powder consists of particles smaller than  $100 \mu\text{m}$  of different shapes, including spherical and flake like morphology. The corresponding magnetization measurement is shown in Figure 3b, in which can be seen a  $M_{3T}$  of  $90 \text{ A} \cdot \text{m}^2/\text{kg}$  and  $H_C$  of 0.12 T. This shows a substantial increase in coercivity from the VIM bulk precursor,  $H_C < 0.03 \text{ T}$ , and a slight decrease in the  $M_{3T}$ . This behavior is commonly attributed to the plastic deformation and strain of the produced powder during the mechanical milling, which is more evident in longer milling procedure, as reported by [7]. It worth mentioning that longer and more intensive milling can be used to produce powder that shows even higher coercivity, reaching values around 0.50 T, but this comes with a decrease in magnetization and even a decomposition of the  $\tau$ -phase, as reported by Law et al. [39].

### 3.3 Suction casting

Through suction casting technique is expected to have a higher cooling rate compared to VIM method. Indeed, as shown in Figure 4a, the microstructure differs from the VIM sample where is observed the presence of three distinct phases:  $\tau$ -,  $\gamma_2$ - and  $\epsilon$ -phases. The  $\epsilon$ -phase arises from the higher cooling compared to VIM, which is also in agreement with the refinement of the  $\tau$ -phase. The high fraction of  $\gamma_2$ -phase present in the sample indicate that further annealing needs to be done to further homogenize and maximize the  $\tau$ -phase fraction. After annealing at  $1100^\circ\text{C}$ , temperature region of  $\epsilon$ -phase stability, for 72 h with subsequently quenching into water, leads to a change in the microstructure, as can be observed in Figure 4b. In the outer shell of the cylindrical sample is observed the

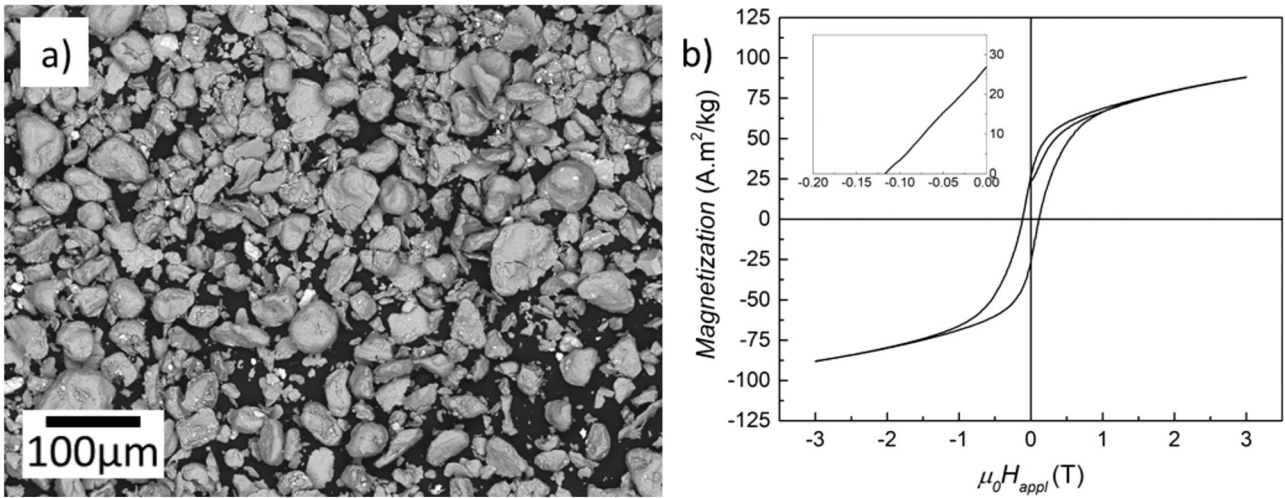


Fig. 3. SEM-BSE image of the produced Mn-Al-C powder (a) and the corresponding magnetization measurements (b).

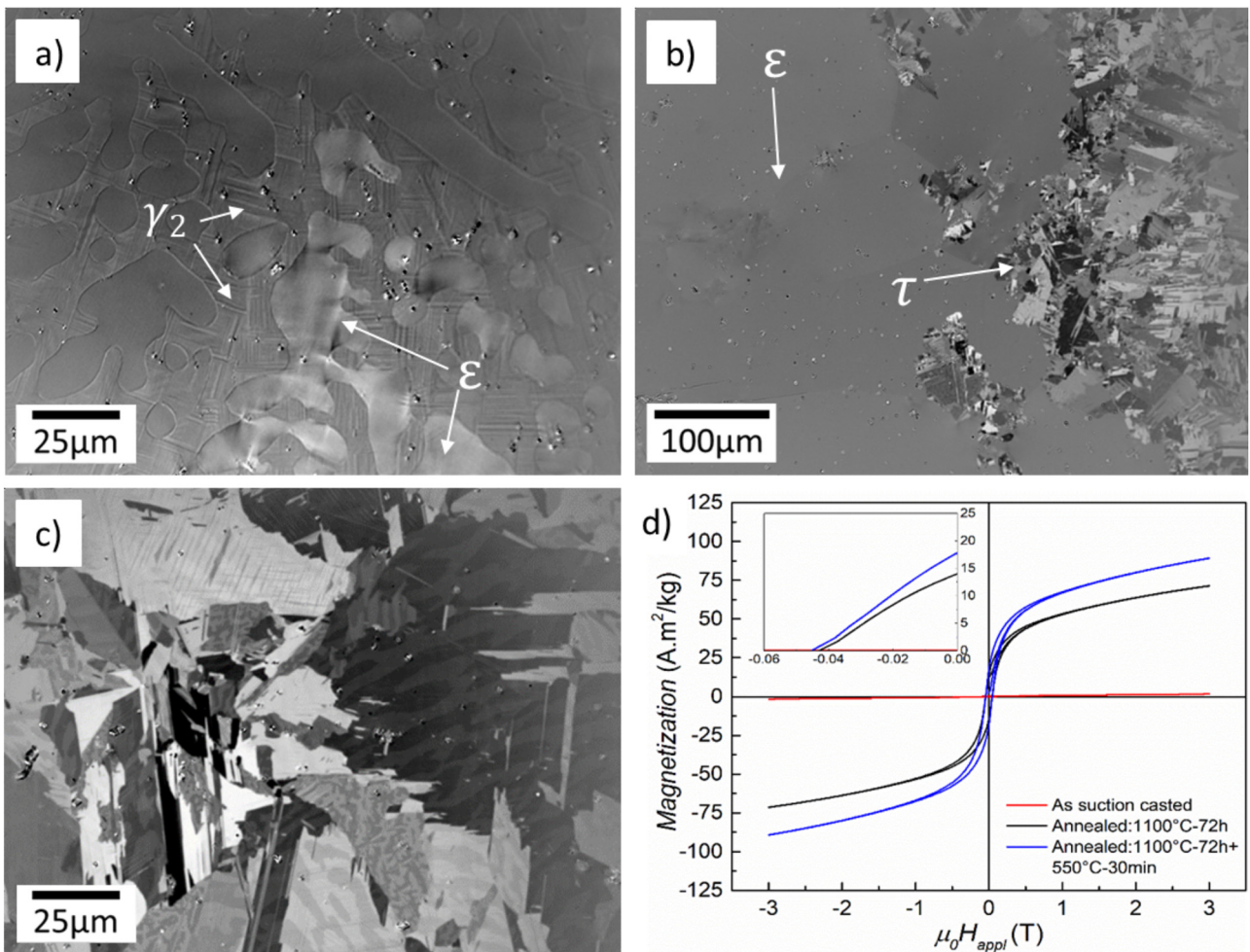
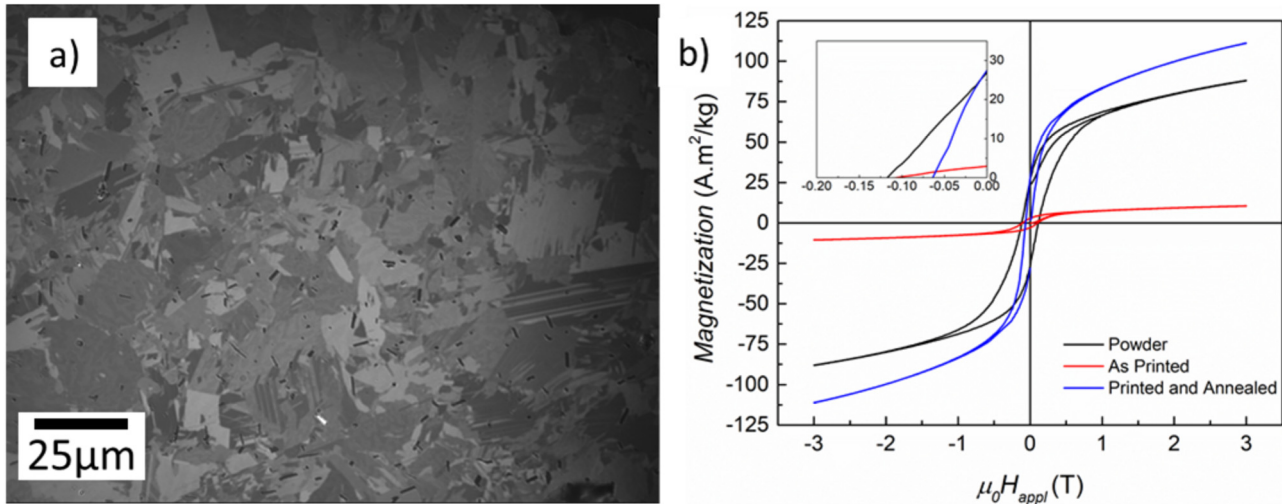


Fig. 4. Kerr images illustrating the microstructure of suction-casted sample in the as cast state (a), after annealing at 1100 °C for 72 h (b) and after annealing at 1100 °C for 72 h and 550 °C for 30 min and the corresponding magnetization measurements (d). The EDS of γ<sub>2</sub>-phase has shown Mn<sub>50</sub>Al<sub>50</sub> composition.



**Fig. 5.** Mn-Al-C sample produced by EBM (a) Kerr image preprocessed sample, showing the  $\tau$  phase is predominantly present and (b) magnetization measurement of the initial powder, the EBM samples and the EBM samples after post-processing.

presence of  $\varepsilon$ -phase because of the higher quenching rate on the edges of the sample, while in the interior we observe the  $\tau$ -phase. To further maximize the ferromagnetic phase fraction, an additional annealing step at 550 °C for 30 min was adopted, which led to a microstructure of pure  $\tau$ -phase, as can be seen in the Figure 4c and from the magnetization values in Figure 4d. Similar to the VIM sample, features like twin boundaries and micro twins are observed in the microstructure.

Accordingly, the magnetization measurements shown in Figure 4d agrees well with the microstructure observation. In the as suction casted state, small fraction of  $\tau$ -phase, the low magnetization represents the non-magnetic  $\gamma_2$ - and  $\varepsilon$ -phases, which are in large fraction in this state. By annealing at 1100 °C, there is an increasing the  $\tau$ -phase fraction and the change on the curve shape to a ferromagnetic behavior with coercivity around 0.04 T and  $M_{3T}$  of 70 A · m<sup>2</sup>/kg. After annealing at 550 °C, we promote the  $\varepsilon \rightarrow \tau$  transformation, leading to a higher ferromagnetic phase fraction resulting in a higher magnetization ( $M_{3T}$  of 90 A · m<sup>2</sup>/kg) with similar coercivity. It is worth to mention that only a slight increase in the coercivity value was observed from the suction casted sample when compared to the VIM sample, from below 0.03 T to around 0.04 T.

### 3.4 Beam-based powder bed additive manufacturing

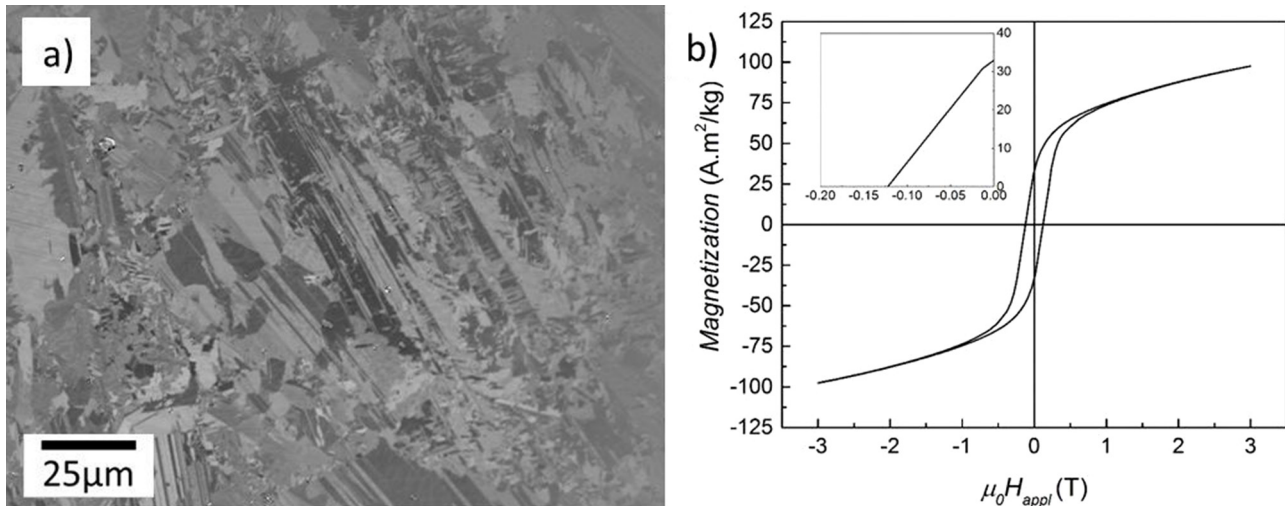
The part of the current work devoted on the Additive Manufacturing of MnAl-C magnets by Beam-based Powder Bed technology is a continuation of the work published previously [14] and [15], where ball milled binary Mn-Al alloy was used as a precursor. The samples were printed using a modified ArcamA2 EBM machine and ball-milled Mn-Al-C alloy with particles size of 50–60 μm (see Fig. 1). As already discussed above, the use of C doped powder was expected to improve the phase stability and enhance the magnetic properties of the printed magnets. The experiment has shown that contrary to the induction

melting process, after electron beam melting the magnetic  $\tau$ -phase is not predominant. This can be due to the use of not optimal process parameter settings like scanning rate, hatching distance, process temperature, etc. Therefore, further investigation of the influence of process parameter settings on the microstructure forming aspects responsible for formation of proper magnetic properties should be done. On another hand, the amount of  $\tau$ -phase in the printed samples can be increased by post processing. Magnetization measurements confirmed (Fig. 5) that the properties of the printed magnets can be fully recovered by two step annealing at 1100 and 500 °C. However, the properties cannot be further improved.

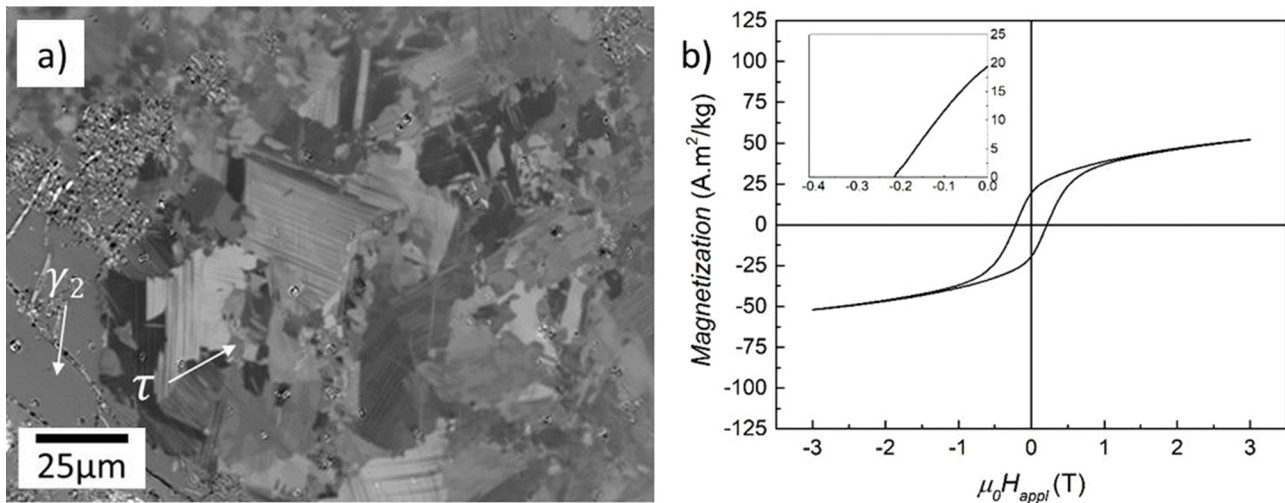
### 3.5 Hot extrusion/deformation and hot pressing

Figure 6a and b presents the microstructure and magnetic properties of the hot deformed (slightly extruded) Mn-Al-C sample, respectively. It can be observed that the hot deformation has caused dynamic recrystallization, which explains the microstructure refinement while preserving the  $\tau$ -phase which can be also observed by the high  $M_{3T}$  value of 97 A · m<sup>2</sup>/kg. The coercivity value has substantially increase when compared to the previous processing routes, going from 0.03 to 0.12 T. This shows that the combination of grain refinement and the induced defects during plastic deformation, such as dislocation, can improve coercivity without affecting the magnetization, which is in agreement to results reported by Thielsch et al. [9] and Feng et al. [37].

As it was mentioned above, because of the brittle nature of this compound, the sample has been deformed and only slightly extruded at the beginning of the extrusion die. This show that the extrusion temperature of 500 °C was not enough to induce plasticity for deformation process, but, as mentioned previously, higher temperatures could lead to decomposition of the metastable ferromagnetic phase. For this reason, a further detailed study on the influence of



**Fig. 6.** Kerr micrograph of the hot-deformed sample (slightly extruded) Mn-Al-C sample (a) and the corresponding magnetization measurement (b).



**Fig. 7.** Kerr image of the hot-pressed Mn-Al-C sample (a) showing the two present phases ( $\gamma_2$  and  $\tau$ -phases) and the magnetization measurement (b). The EDS of  $\gamma_2$ -phase has shown  $\text{Mn}_{49}\text{Al}_{51}$  composition.

chemical composition, process temperature, phase stabilization and magnetic properties would give an insight of the processing window for this material system, but this is beyond the scope of the present work.

Alternatively, with the aim to overcome the technical difficulties presented during the hot extrusion route and produce a refined  $\tau$ -phase microstructure, the hot compaction of the produced ball milled powder has been performed. The obtained hot-compacted samples had the microstructure as shown in Figure 7a. As can be seen, the metastable phase partially was decomposed during the process, but the remaining  $\tau$ -phase shows a refined microstructure when compared to VIM and suction casting processes. It is important to notice that was observed porosity in this sample, which led to a sample with density of  $4,3\text{g/cm}^3$ , around 83% relative to the theoretical density, measure by Archimedes' principle.

The magnetization curve of the hot-pressed sample, Figure 7b, shows a magnetization  $M_{3T}$  of  $50\text{ A}\cdot\text{m}^2/\text{kg}$ , related to a decrease of the ferromagnetic phase fraction. On the other hand, the coercivity has improved, reaching a value of  $0.21\text{ T}$ , showing again, as in the case of hot extrusion, that grain refinement and defects induced during the process contribute to improve this property.

### 3.6 High pressure torsion – severe plastic deformation

Another deformation processing route that has been investigated in this work was high pressure torsion (severe plastic deformation), but different from the 295 previous ones, the deformation was carried out at room temperature. As can be seen from the magnetization measurements, Figure 8c, there is a gradient on the coercivity and magnetization values across the diameter. The increase in

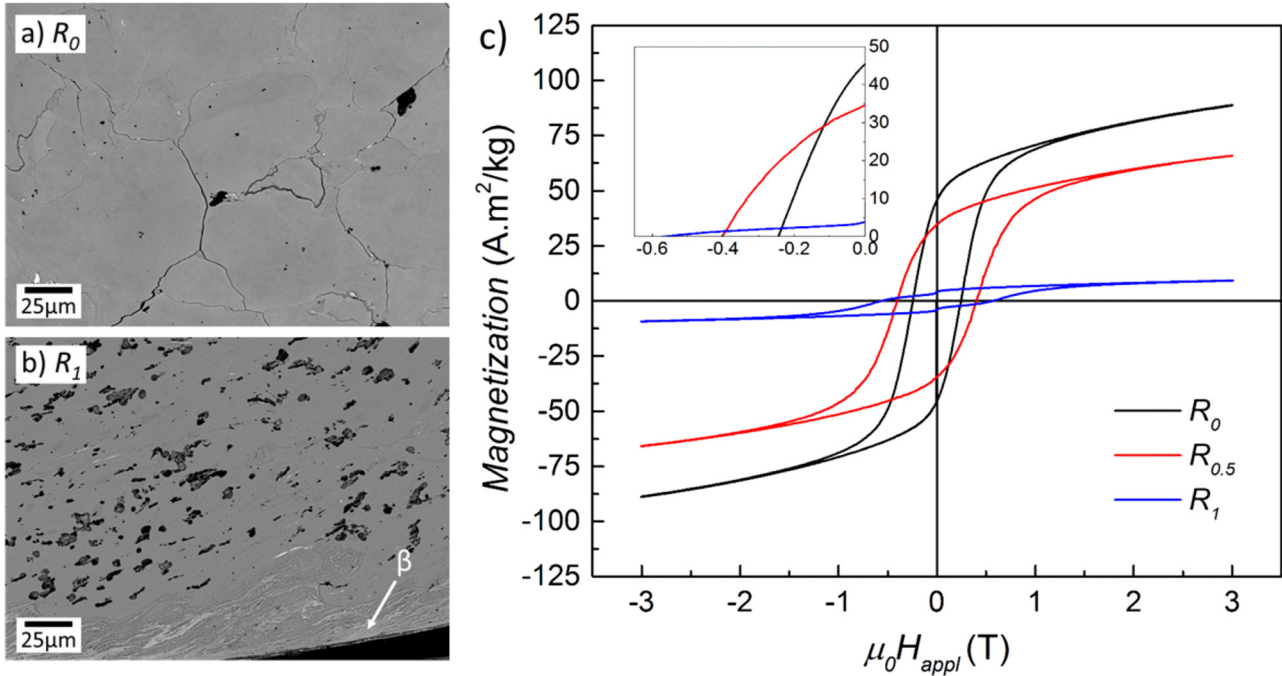


**Fig. 8.** SEM-BSE images showing the microstructure in the center (a)- $R_0$  and on the edge (b)- $R_1$  of high pressure deformed sample and magnetization measurements of different regions of the sample (c). The EDS of  $\beta$ -phase has shown  $Mn_{64}Al_{36}$  composition.

the coercivity towards the edge of the sample ( $R_1$ ), from 0.22 to 0.58 T, can be associated to the higher strain that this area is subjected during the HPT process and, consequently, higher defect density. The high values of coercivity obtained by HPT are similar to the ones reported by other authors and also similar for powders produced by high energy ball milling, in which the powder is also subjected to high a deformation degree.

On the other hand, the magnetization value decreases because of higher Mn-Mn antiferromagnetic interaction caused by internal stresses, which has been shown also for other processing routes [8]. In addition to the decrease in the absolute magnetization value, it is possible to notice a step-like decrease in the magnetization value. This behavior is related to the appearance of secondary phase caused by the stress-driven decomposition of the metastable  $\tau$ - into  $\beta$ -phase, as confirmed by SEM-EDS (see Fig. 8b). The nucleated phase also contributes to the decrease in the absolute magnetization value since it is nonmagnetic.

To correlate the obtained magnetic results with microstructure, SEM analysis were made in the center ( $R_0$ -Fig. 8a) and at the edges ( $R_1$ -Fig. 8b), revealing a gradient on the microstructure morphology. Kerr microscopy was also used but it was not possible to distinguish features, like grain size or twins, as shown for the previous processing routes. For this reason, TEM analysis was carried in the as cast (VIM), powder precursor and in the HPT ( $R_1$  region) states, as shown in Figure 9. In the as cast state (VIM), as shown previously in Figure 2a and also in Figure 9a, the microstructure is composed from coarse grains (micrometer range) with well-defined twins and twin

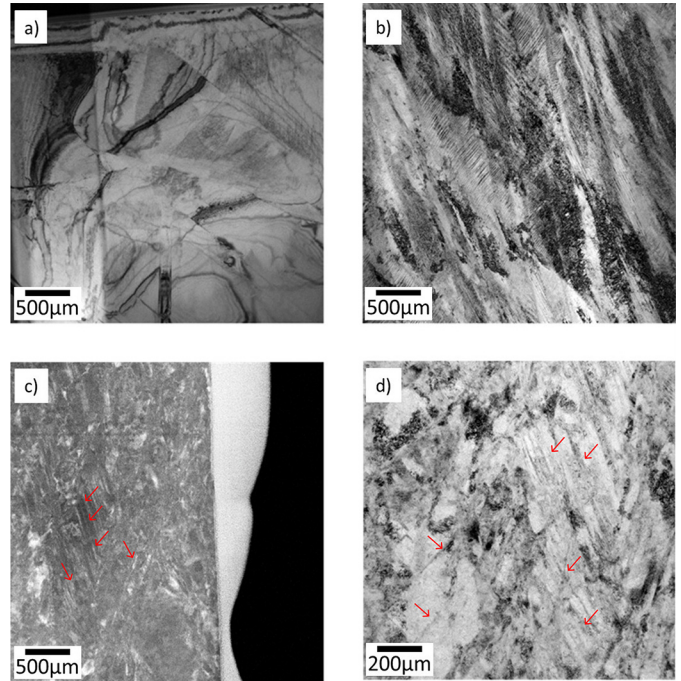


**Fig. 9.** HR-TEM of the Mn-Al-C samples in different states for comparison: (a) VIM, (b) powder precursor for HPT and (c, d) after HPT.

boundaries. As for the powder, Figure 9b, it is possible to notice a difference in the morphology and size of the grains along the presence with a higher density of defects.

**Table 1.** Various fabrication techniques of Mn-Al-based permanent magnets and their main magnetic characteristics.

| Fabrication technique | $H_c$ (kOe) | $M_r$ (A · m <sup>2</sup> /kg) | $M_S$ (A · m <sup>2</sup> /kg) | Ref.               |
|-----------------------|-------------|--------------------------------|--------------------------------|--------------------|
| Induction melting     | 0.3         | 17.5                           | 100.0                          | This work          |
|                       | 0.2         | 23.0                           | 120.0                          | [8]                |
| Arc melting           | –           | –                              | –                              | This work          |
|                       | 0.1         | 5.0                            | n.i.                           | [38]               |
| Suction cast          | 0.4         | 18                             | 90                             | This work          |
|                       | –           | –                              | –                              | –                  |
| Hot compacted         | 2.2         | 20                             | 50                             | This work          |
|                       | 3.3         | 28                             | 50                             | [19]               |
| Hot deformed          | –           | –                              | –                              | This work          |
|                       | 2.2         | 50                             | 82                             | [19]               |
| Hot extruded          | 1.2         | 32                             | 97                             | This work          |
|                       | 3.2         | 85.7                           | 111.2                          | [37]               |
| Spark plasma sintered | –           | –                              | –                              | This work          |
|                       | 2.4         | 12.0                           | 28                             | [44]               |
| FDM printed           | –           | –                              | –                              | This work          |
|                       | 1.53        | 35.8                           | 80.0                           | [16]               |
| EBM printed           | 0.6-1.2     | 3.1-26.3                       | 10.7-111.3                     | This work and [15] |
|                       | –           | –                              | –                              | –                  |
| High pressure torsion | 2.5-5.8     | 5.0-45.0                       | 10.0-90.0                      | This work          |
|                       | 5.9         | 15.0                           | 40.0                           | [30]               |

The abbreviation “n.i.” means that this information was not provided by the authors.

The sample after HPT, Figure 9c and d, shows even further microstructural refinement and change in morphology, being difficult to distinguish individual grains. But it is noticeable the increase of defect density, including polytwinned microstructure with high density of dislocations. The high density of defects, especially dislocations, can hinder the domain wall motion leading to a higher coercivity, in accordance with the magnetic results presented in Figure 8c, and as previous reported by [30,31,41].

The results indicate that the coercivity is strongly related to the defects, and the density of such defects, that can pin the domain wall motion in the magnetization reversal process. Even though plastic deformation/severe plastic deformation is beneficial for this figure of merit, the magnetization value decreases due to internal stresses, as seen and explained previously. For this reason, a compromise between these two properties can be established by using HPT or even with the addition post annealing processing step. These possibilities can be further studied and explored to achieve a balanced magnet in terms of magnetization and coercivity, but the absence of texture coming from the HPT still remains a challenge for increasing remanence and, consequently, the energy-product  $BH_{max}$ .

Table 1 summarizes the magnetic characteristics of Mn-Al-C permanent magnets produced by various techniques that were found in literature. The results of the experimental findings presented in this work were also added to the Table 1 for comparison.

## 4 Conclusion

To investigate the influence of different production methods of bulk Mn-Al-C based permanent magnets on their magnetic properties, a batch of Mn<sub>52</sub>Al<sub>46</sub>C<sub>2</sub> precursor alloy was prepared by vacuum induction melting for further processing. MnAl based permanent magnets were produced by applying different degree of mechanical deformation and heat treatment. The resulting permanent magnets were studied with respect of the correlation between microstructure and magnetic properties.

It was clearly shown that the phase purity of the samples is important, but not the ultimate factor determining the magnetic properties of the MnAlC samples. Beside the amount of  $\tau$ -phase, the density and the type of microstructural defects can significantly affect the extrinsic magnet properties of this material system. The samples that were subject of plastic deformation during the manufacturing process (hot extrusion, high pressure torsion and milling) have higher defects density. By having these higher defect density, especially dislocations, high coercivity values were obtained because these defects can act as pinning center than can hinder the reversal domains movement. On the other hand, the strain related to these processes can reduce magnetization due to Mn-Mn antiferromagnetic interaction and, in some cases, can also leads to a decomposition of the ferromagnetic metastable  $\tau$ -phase.

Techniques related to melting with slow cooling (VIM) or with post annealing processing (suction casting) have

shown the highest magnetization values. Based on the obtained results, it can be concluded that introducing texture along the easy magnetization axis can (without negative effect on the magnetization) maximize the remanence and consequently the energy product  $BH_{max}$  of the magnets. From all investigated methods, as previously reported, only samples produced by hot extrusion has shown a significant degree texturing. Due to the experimental constraints (temperature and pressure), this could not be fully reproduced and therefore only isotropic samples are reported in this work.

Among the explored techniques, hot extrusion and high pressure torsion have shown promising possibilities to further develop Mn-Al-C as permanent magnets. However, it should be taken into account the challenges related to design a proper processing window for hot extrusion and the limitation of HPT regarding the absence of texture.

This work was supported by the European Union's Horizon 2020 NMBP232015 research No 686056 (NOVAMAG). F.Maccari acknowledges the funding provided by the Deutsche Forschungsgemeinschaft DFG (German Research Foundation) under the Priority Programme SPP1959-Fields Matter.

## References

1. A.J.J. Koch, P. Hokkeling, M.G.v.d. Steeg, K.J. de Vos, New material for permanent magnets on a base of Mn and Al, *J. Appl. Phys.* **31** (1960) S75–S77
2. J. Cui, M. Kramer, L. Zhou, F. Liu, A. Gabay, G. Hadjipanayis, B. Balasubramanian, D. Sellmyer, Current progress and future challenges in rare-earth-free permanent magnets, *Acta Mater.* **158** (2018) 118–137
3. K. Patel, J. Zhang, S. Ren, Rare-earth-free high energy product manganese-based magnetic materials, *Nanoscale* **10** (2018) 11701–11718
4. K.P. Skokov, O. Gutfleisch, Heavy rare earth free, free rare earth and rare earth free magnets – Vision and reality, *Scr. Mater.* **154** (2018) 289–294
5. A.E. Berkowitz, J.D. Livingston, J.L. Walter, Properties of Mn-Al-C magnets prepared by spark erosion and other rapid solidification techniques, *J. Appl. Phys.* **55** (1984) 2106–2108
6. A. Chaturvedi, R. Yaqub, I. Baker, Microstructure and magnetic properties of bulk nanocrystalline MnAl, *Metals* **4** (2014) 20–27
7. H. Jian, K.P. Skokov, O. Gutfleisch, Microstructure and magnetic properties of Mn-Al-C alloy powders prepared by ball milling, *J. Alloys Compd.* **622** (2015) 524–528
8. F. Bittner, J. Freudenberger, L. Schultz, T.G. Woodcock, The impact of dislocations on coercivity in  $L1_0$ -MnAl, *J. Alloys Compd.* **704** (2017) 528–536
9. J. Thielsch, F. Bittner, T.G. Woodcock, Magnetization reversal processes in hot-extruded  $\tau$ -MnAl-C, *J. Magn. Mater.* **426** (2017) 25–31
10. S. Bance, F. Bittner, T.G. Woodcock, L. Schultz, T. Schrefl, Role of twin and anti-phase defects in MnAl permanent magnets, *Acta Mater.* **131** (2017) 48–56
11. F. Bittner, L. Schultz, T.G. Woodcock, The role of the interface distribution in the decomposition of metastable  $L1_0$ - $Mn_{54}Al_{46}$ , *J. Alloys Compd.* **727** (2017) 1095–1099
12. R. Madugundo, G.C. Hadjipanayis, Anisotropic Mn-Al-(C) hot-deformed bulk magnets, *J. Appl. Phys.* **119** (2016) 013904
13. A.M.G. Unalan, Development of rare-earth free permanent magnets, Ph.D. thesis, Graduate School of Natural and Applied Sciences of Middle East Technical University (2017). [etd.lib.metu.edu.tr/upload/12621677/index.pdf/123456789/26977](http://etd.lib.metu.edu.tr/upload/12621677/index.pdf/123456789/26977)
14. V. Popov, A. Koptuyug, I. Radulov, F. Maccari, G. Muller, Prospects of additive manufacturing of rare-earth and non-rare-earth permanent magnets, *Procedia Manuf.* **21** (2018) 100–108
15. I.A. Radulov, V.V. Popov, A. Koptuyug, F. Maccari, A. Kovalevsky, S. Essel, J. Gassmann, K.P. Skokov, M. Bamberger, Production of net-shape Mn-Al permanent magnets by electron beam melting, *Addit. Manuf.* **30** (2019) 100787
16. E.M. Palmero, J. Rial, J. de Vicente, J. Camarero, B. Skårman, H. Vidarsson, P.O. Larsson, A. Bollero, Development of permanent magnet MnAlC/polymer composites and flexible filament for bonding and 3D-printing technologies, *Sci. Technol. Adv. Mater.* **19** (2018) 465–473
17. Z.W. Liu, C. Chen, Z.G. Zheng, B.H. Tan, R.V. Ramanujan, Phase transitions and hard magnetic properties for rapidly solidified MnAl alloys doped with C, B, and rare earth elements, *J. Mater. Sci.* **47** (2011) 2333–2338
18. J.M.D. Coey, Permanent magnets: plugging the gap, *Scr. Mater.* **67** (2012) 524–529
19. R. Madugundo, O. Koylu-Alkan, G.C. Hadjipanayis, Bulk Mn-Al-C permanent magnets prepared by various techniques, *AIP Adv.* **6** (2016) 056009
20. R.W. McCallum, L. Lewis, R. Skomski, M.J. Kramer, I.E. Anderson, Practical aspects of modern and future permanent magnets, *Ann. Rev. Mater. Res.* **44** (2014) 451–477
21. F. Bittner, L. Schultz, T.G. Woodcock, Twin-like defects in  $L1_0$  ordered  $\tau$ -MnAl-C studied by EBSD, *Acta Mater.* **101** (2015) 48–54
22. S. Zhao, Y. Wu, Z. Jiao, Y. Jia, Y. Xu, J. Wang, T. Zhang, C. Jiang, Evolution of intrinsic magnetic properties in  $L1_0$  Mn-Al alloys doped with substitutional atoms and correlated mechanism: experimental and theoretical studies, *Phys. Rev. Appl.* **11** (2019) 64008
23. V. Øygarden, J. Rial, A. Bollero, S. Deledda, Phase-pure  $\tau$ -MnAlC produced by mechanical alloying and a one-step annealing route, *J. Alloys Compd.* **779** (2019) 776–783
24. D. Palanisamy, D. Raabe, B. Gault, Elemental segregation to twin boundaries in a MnAl ferromagnetic Heusler alloy, *Scr. Mater.* **155** (2018) 144–148
25. J.M.K. Wiezorek, A.K. Kulovitz, C. Yanar, W.A. Soffa, Grain boundary mediated displacive-diffusional formation of  $\tau$ -phase MnAl, *Metall. Mater. Trans. A* **42** (2011) 594–604
26. P.-Z. Si, H.-D. Qian, C.-J. Choi, J. Park, S. Han, H.-L. Ge, K. P. Shinde, In situ observation of phase transformation in MnAl(C) magnetic materials, *Materials* **10** (2017) 1016
27. H. Zijlstra, H.B. Haanstra, Evidence by Lorentz microscopy for magnetically active stacking faults in MnAl alloy, *J. Appl. Phys.* **37** (1966) 2853–2856
28. C. Yanar, J.M.K. Wiezorek, W.A. Soffa, V. Radmilovic, Massive transformation and the formation of the ferromagnetic  $L1_0$  phase in manganese-aluminum-based alloys, *Metall. Mater. Trans. A* **33** (2002) 2413–2423

29. J. Landuyt, G. Tendeloo, J.J. Broek, H. Donkersloot, H. Zijlstra, Defect structure and magnetic properties of MnAl permanent magnet materials, *IEEE Trans. Magn.* **14** (1978) 679–681
30. P.Z. Si, J.T. Lim, J. Park, H.H. Lee, H. Ge, H. Lee, S. Han, H. S. Kim, C.J. Choi, High coercivity in MnAl disc prepared by severe plastic deformation, *Phys. Status Solidi (b)* **257** (2019) 1900356
31. Y. Jia, Y. Wu, S. Zhao, S. Zuo, K.P. Skokov, O. Gutfleisch, C. Jiang, H. Xu,  $L1_0$  rare-earth-free permanent magnets: the effects of twinning versus dislocations in Mn-Al magnets, *Phys. Rev. Mater.* **4** (2020) 94402
32. P. Zhao, L. Feng, K. Nielsch, T.G. Woodcock, Microstructural defects in hot deformed and as-transformed  $\tau$ -MnAl-C, *J. Alloys Compd.* **852** (2021) 156998
33. X.H. Tan, H. Xu, Q. Bai, W.J. Zhao, Y.D. Dong, Magnetic properties of Fe-Co-Nd-Y-B magnet prepared by suction casting, *J. Non Cryst. Solids* **353** (2007) 410–412
34. Z. Yuyong, P. Jing, J. Xiaoli, L. Xincai, D. Youren, X. Xiaoyan, Microstructure evolution and magnetic properties of the  $Nd_9Fe_{81-x}Ti_4C_2Nb_4B_x$  ( $x = 11, 13, 15$ ) bulk magnets prepared by copper mold suction casting, *J. Rare Earths* **33** (2015) 1081–1086
35. F. Maccari, L. Schafer, I. Radulov, L.V.B. Diop, S. Ener, E. Bruder, K. Skokov, O. Gutfleisch, Rapid solidification of  $Nd_{1+x}Fe_{11}Ti$  compounds: phase formation and magnetic properties, *Acta Mater.* **180** (2019) 15–23
36. T. Ohtani, N. Kato, S. Kojima, K. Kojima, Y. Sakamoto, I. Konno, M. Tsukahara, T. Kubo, Magnetic properties of Mn-Al-C permanent magnet alloys, *IEEE Trans. Magn.* **13** (1977) 1328–1330
37. L. Feng, J. Freudenberger, T. Mix, K. Nielsch, T.G. Woodcock, Rareearth-free MnAl-C-Ni permanent magnets produced by extrusion of powder milled from bulk, *Acta Mater.* **199** (2020) 155–168
38. N. Singh, V. Mudgil, K. Anand, A.K. Srivastava, R.K. Kotnala, A. Dhar, Influence of processing on structure property correlations in  $\tau$ -MnAl rareearth free permanent magnet material, *J. Alloys Compd.* **633** (2015) 401–407
39. J.Y. Law, J. Rial, M. Villanueva, N. Lopez, J. Camarero, L. G. Marshall, J.S. Blazquez, J.M. Borrego, V. Franco, A. Conde, L.H. Lewis, A. Bollero, Study of phases evolution in high-coercive MnAl powders obtained through short milling time of gas-atomized particles, *J. Alloys Compd.* **712** (2017) 373–378
40. Y. Jia, Y. Wu, S. Zhao, J. Wang, C. Jiang, Relation between solidification microstructure and coercivity in MnAl permanent-magnet alloys, *Intermetallics* **96** (2018) 41–48
41. M.V. Gorshenkov, D.Y. Karpenkov, R.V. Sundeev, V.V. Cheverikin, I.V. Shchetinin, Magnetic properties of Mn-Al alloy after HPT deformation, *Mater. Lett.* **272** (2020) 127864
42. A. Zhilyaev, T. Langdon, Using high-pressure torsion for metal processing: fundamentals and applications, *Prog. Mater. Sci.* **53** (2008) 893–979
43. A.G. Popov, V.S. Gaviko, V.V. Popov, O.A. Golovnia, A.V. Protasov, E.G. Gerasimov, A.V. Ogurtsov, M.K. Sharin, R. Gopalan, Structure and magnetic properties of heat-resistant  $Sm(Co_{0.796-x}Fe_{0.177}Cu_xZr_{0.027})_{6.63}$  permanent magnets with high coercivity, *JOM* **71** (2018) 559–566
44. P. Saravanan, V.T.P. Vinod, M. Černík, A. Selvapriya, D. Chakravarty, S.V. Kamat, Processing of Mn-Al nanostructured magnets by spark plasma sintering and subsequent rapid thermal annealing, *J. Magn. Magn. Mater.* **374** (2015) 427–432

**Cite this article as:** Vladimir V. Popov Jr., Fernando Maccari, Iliya A. Radulov, Aleksey Kovalevsky, Alexander Katz-Demyanetz, Menahem Bamberger, Microstructure and magnetic properties of Mn-Al-C permanent magnets produced by various techniques, *Manufacturing Rev.* **8**, 10 (2021)